Nuclear Inst. and Methods in Physics Research, A 897 (2018) 22–31

Contents lists available at ScienceDirect

Nuclear Inst. and Methods in Physics Research, A

journal homepage: www.elsevier.com/locate/nima

Investigation of neutron interactions with Ge detectors

Miloslava Baginova [a,b,*], Pavol Vojtyla [a], Pavel P. Povinec [b]

[a] CERN, Geneva 1211, Switzerland

[b] Faculty of Mathematics, Physics and Informatics, Comenius University, Mlynská dolina F1, 842 48 Bratislava, Slovakia

ARTICLE INFO

Keywords:
Monte Carlo simulation
Detector background
GEANT4
Neutron interactions
High-purity Ge detectors

ABSTRACT

Interactions of neutrons with a high-purity germanium detector were studied experimentally and by simulations using the GEANT4 tool. Elastic and inelastic scattering of fast neutrons as well as neutron capture on Ge nuclei were observed. Peaks induced by inelastic scattering of neutrons on ^{70}Ge, ^{72}Ge, ^{73}Ge, ^{74}Ge and ^{76}Ge were well visible in the γ-ray spectra. In addition, peaks due to inelastic scattering of neutrons on copper and lead nuclei, including the well-known peak of ^{208}Pb at 2614.51 keV, were detected. The GEANT4 simulations showed that the simulated spectrum was in a good agreement with the experimental one. Differences between the simulated and the measured spectra were due to the high γ-ray intensity of the used neutron source, physics implemented in GEANT4 and contamination of the neutron source.

1. Introduction

Background of high-purity germanium (HPGe) detectors induced by neutrons is a poorly understood component in low-level γ-spectrometry systems. In surface laboratories with passive shielding, as well as in underground laboratories, neutrons can be produced by interactions of high energy cosmic rays and by natural radionuclides in spontaneous fission and in (α, n) reactions. Predicting all background components correctly is crucial for designing efficient shielding and applying appropriate event-rejection strategies.

The suppression and rejection of background is one of the key issues in experiments looking for rare nuclear events, such as neutrinoless $\beta\beta$ decay experiments, dark matter searches or experiments with low-energy neutrinos. Monte Carlo simulations of neutron background play a crucial role in evaluation of the total background and for the optimization of rejection strategies (e.g. [1,2]).

No study with a complex information about neutron background has been available till now, however, several studies were dealing with neutron interactions with germanium detectors. The knowledge of germanium peak shapes is important because they could cause systematic errors. Past measurements of neutron interactions with Ge detectors were carried out using ^{252}Cf neutron sources and environmental neutrons (e.g. [3,4]). A comparison of results showed that there is no substantial difference between Ge experimental peaks with a wide spectrum of neutron energies. The broader germanium peaks were observed for high energy neutrons [4].

The energy deposition process of the recoiling Ge nuclei has been studied, as well as elastic scattering of neutrons with Ge detectors [4,5]. Monte Carlo simulations of ^{252}Cf induced γ-ray spectra in Ge detectors were also carried out, and a good agreement of simulated spectra with experimental ones was found, especially for the region of elastic neutron scattering up to 50 keV. However, no detail analysis of experimental γ-ray spectra was carried out till now. As such investigations are crucial for determination of all Ge background components (especially in underground laboratories), we decided to carry out analysis of ^{241}Am–Be neutron induced γ-ray spectra both experimentally, as well as by Monte Carlo simulations.

2. Experimental setup

2.1. ^{241}Am–Be source

In order to investigate neutron-induced background, interactions of neutrons with a Ge detector were studied experimentally as the first step. Monte Carlo simulations using the GEANT4 simulation tool developed at CERN [6–9] were carried out as the next.

The ^{241}Am–Be source with a nominal activity of 370 MBq was used as a neutron source in the experiment. The source was produced in 2009 and its working life is 15 years. It contained compacted mixture of powders of ^{241}Am oxide and ^{9}Be. The neutron intensity in 2016 was about 23 000 neutrons s^{-1}. The standard neutron spectrum has the average and the maximal neutron energies of 4.2 and 11 MeV, respectively [10,11]. Neutrons are produced in ^{9}Be(α, n)^{12}C reactions,

* Corresponding author at: CERN, Geneva 1211, Switzerland.
E-mail address: miloslava.baginova@cern.ch (M. Baginova).

https://doi.org/10.1016/j.nima.2018.04.036
Received 11 December 2017; Received in revised form 13 April 2018; Accepted 18 April 2018
Available online 25 April 2018

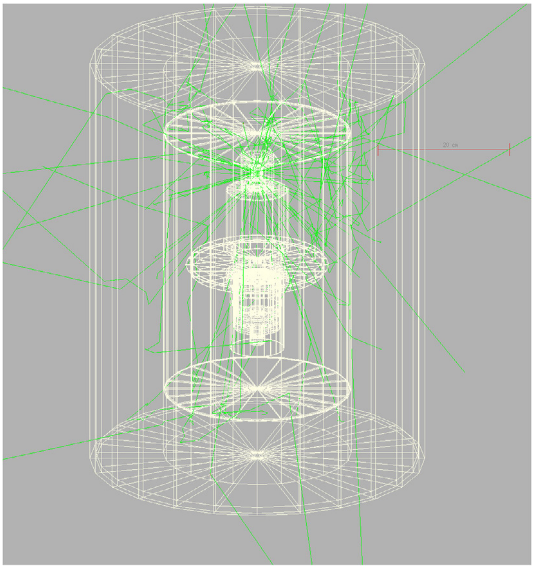

Fig. 1. Experimental setup with several simulated neutron and γ-ray interactions.

which are accompanied by emission of 4.44 MeV γ-rays from excited ^{12}C daughter nuclei. The shape of the neutron source is a cylinder with a diameter of 14 mm and a length of 12 mm. The active part was encapsulated in a case made of stainless steel and an aluminium shell.

2.2. Ge detector

The experimental setup consisted of an ^{241}Am–Be source placed coaxially 161.2 mm above a Canberra coaxial p-type Ge detector with a relative efficiency of 50%. The germanium crystal with a diameter of 66 mm and a height of 59 mm was enclosed in a thermoplastic foil and in an aluminium cryostat with a copper crystal holder. The cavity inside the crystal was 10 mm in diameter and 45 mm in height. The energy resolution of the detector was 2.07 keV for 1332.40 keV γ-rays of ^{60}Co. The energy calibration of the detector was done with ^{60}Co source. The detector efficiency calculation was done using LabSOCS software from Canberra. Two circular iron absorbers were placed above the detector to absorb abundant but low-energy γ-rays of ^{241}Am with the aim to reduce the dead time of the detector. A plastic beaker was used to place the source at a certain distance from the detector to further reduce the dead time and to minimize the energy summation effect. In this way, a dead time correction of only about 12.6% could be reached. The source–detector setup was placed in a shield consisting of 9.5 mm of carbon steel, 102 mm of lead, 1 mm of tin foil and 1.5 mm of copper cladding (from outside to inside). The outer shield dimensions were 508 mm in diameter and 635 mm in height. The γ-energy spectrum ranged from 10 to 3000 keV. Typical measuring time was 25 h. The background γ-spectrum (without ^{241}Am–Be source) was measured as well, and it was subtracted from measured neutron induced γ-spectra. A low nominal activity of the neutron source and short measuring time did not produce any neutron damage of the detector. The arrangement, as implemented in the GEANT4 simulation code is illustrated in Fig. 1.

2.3. Energy deposition mechanism

The principal energy deposition mechanisms of neutrons with energies up to 11 MeV in the Ge detector are elastic and inelastic scattering. The elastic scattering of neutrons gives the largest contribution to the interaction probability for Ge detector energy up to 50 keV [3]. The dominant process for slow and thermal neutrons is the neutron capture, for fast neutrons the dominant processes are elastic and inelastic scattering, as indicated by cross sections of these reactions discussed below.

Table 1
Composition of natural germanium.

Isotopes	^{70}Ge	^{72}Ge	^{73}Ge	^{74}Ge	^{76}Ge
Abundance (%)	20.52	27.45	7.76	36.52	7.75
Number of neutrons	38	40	41	42	44

Natural germanium used in the detector is composed of 5 naturally occurring isotopes (Table 1). The purity of Ge crystals is usually at least 99.999%.

Cross sections for interactions of neutrons with germanium isotopes are shown in Fig. 2. They have common features, but different quantitative parameters as follows. For ^{70}Ge, the neutron capture dominates up to about 1.3 meV where elastic scattering gains significance until the resonance region extending from about 1 to 14 keV. In the resonance region, the cross sections fluctuate sharply within the same amplitude for both neutron capture and elastic scattering, however, the baseline for the elastic scattering may be several orders of magnitude higher. Beyond the resonance region, the elastic scattering takes over again. The inelastic scattering channel opens at about 1 MeV and drops sharply beyond about 10 MeV, the binding energy of a nucleon in a target nucleus. In the energy region of 1−10 MeV, elastic and inelastic scattering concur. However, around 3.5−4.5 MeV, the inelastic scattering is more probable.

For ^{72}Ge, elastic scattering starts to predominate at 0.3 meV. The resonance region extends from 2 keV to 11 keV. There are two strong resonances for the neutron capture below 2 keV. The inelastic scattering cross section predominates from 2.8 to 4.5 MeV.

For ^{73}Ge, the neutron capture predominates up to about 200 meV. The resonance region ranges from about 0.1 keV to 9 keV. The inelastic scattering channel opens at 13 keV but its cross-section becomes comparable to that of elastic scattering only at about 1.8 MeV. Nevertheless, from 2 to 4.5 MeV clearly predominates.

For ^{74}Ge, elastic scattering starts to predominate at about 0.13 meV. The resonance region is very narrow, 2.5–6 keV. Beyond the resonance region, the courses of cross-sections are very similar to those for ^{70}Ge and ^{72}Ge. The inelastic scattering is the most probable process from 2.4 to 4.5 MeV.

Finally, for ^{76}Ge, elastic scattering starts to dominate at 0.01 meV. Several isolated resonances are present in the region from 0.5 keV to 35 keV and the rest is similar to other stable Ge isotopes except for ^{73}Ge. The inelastic scattering channel opens at 0.6 MeV and becomes dominant for 2.5–4.5 MeV.

At neutron energies from 3.5 to 4.5 MeV, the inelastic scattering is the most probable interaction of neutrons with all naturally occurring germanium isotopes. This process is of interest for the background induction by fast neutrons as will be shown later. Let us recall that the elastic scattering of neutrons on Ge nuclei can contribute to the γ-spectrum only below 50 keV [3].

2.4. Monte Carlo simulation

GEANT4 developed at CERN for simulation of particle interactions with matter [6–9] was used for Monte Carlo simulations of interactions of neutrons with a Ge detector. It is based on C++ programming language with object-oriented programming features applicable for particle transport simulations in high as well as low-energy physics. It covers all relevant physical processes, including processes with γ-rays and neutrons. Cross sections for corresponding processes were taken from corresponding data files. For γ-ray interactions G4EMLOW 6.5 and for neutron interactions G4NDL 4.5 data files were used, respectively. The experimental neutron spectrum of the ^{241}Am–Be source was taken from [13]. The spectrum was digitized (Fig. 3) and used as the input source for GEANT4 simulations, together with γ-rays emitted by ^{241}Am and those generated in nuclear reactions inside the source.

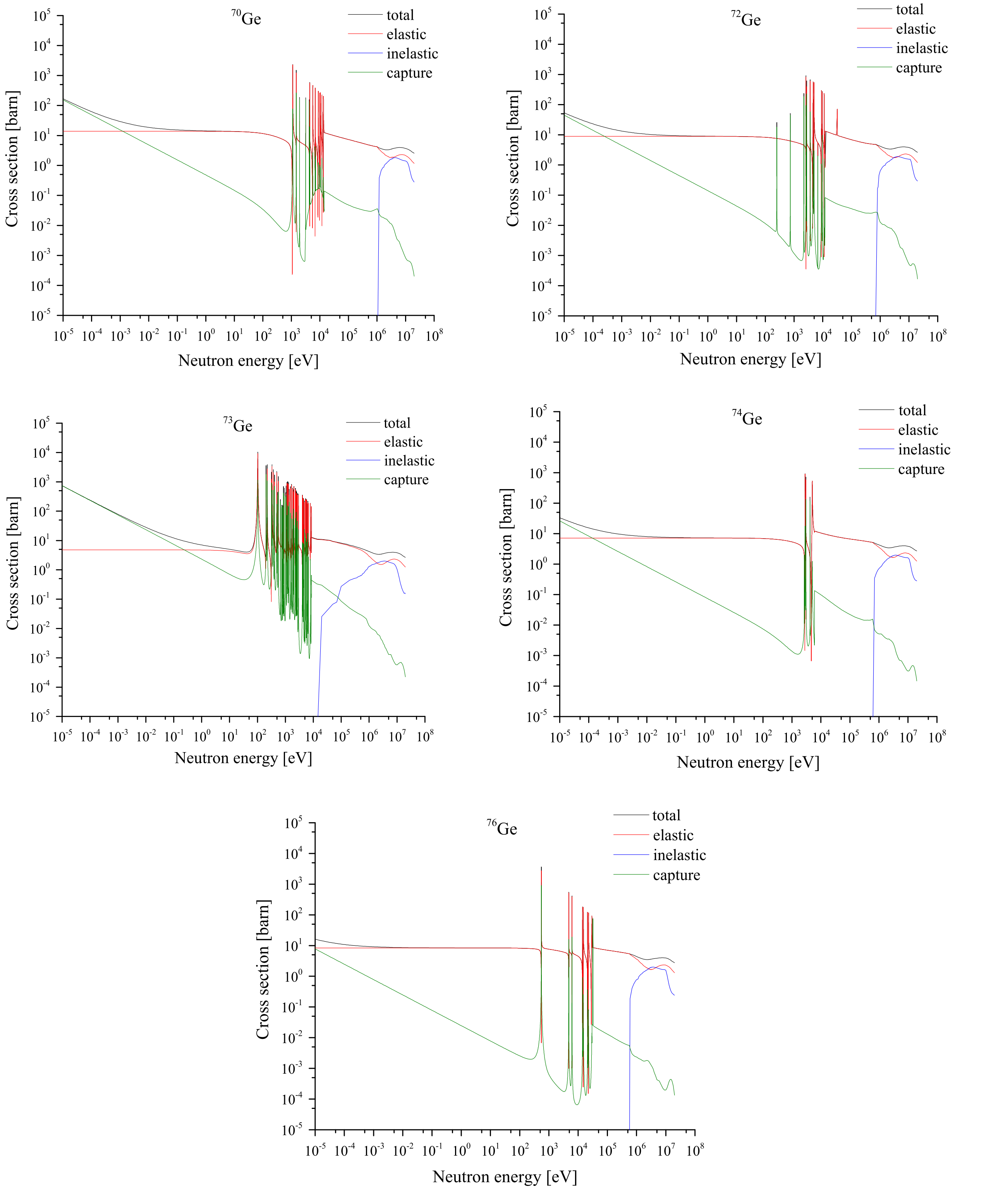

Fig. 2. Calculated cross sections for elastic and inelastic scattering and neutron capture in ^{70}Ge, ^{72}Ge, ^{73}Ge, ^{74}Ge, and ^{76}Ge.
Source: Data taken from JENDL 4.0 database [12].

Gaussian energy distribution was used for γ-rays of ^{241}Am and γ-rays from ^{9}Be(α, n)^{12}C reaction with mean energies of 59.54 keV and 4438.91 keV, with standard deviations of 0.24 keV and 1.55 keV, respectively. Values of mean energies were taken from NuDat 2.6 database [14], and values of standard deviations were taken from the energy resolution of the Ge detector (Fig. 4), which was measured using radioactive standards and the resolution curve was calculated using the least square method. The resolution curve was then approximated up to 5 MeV. The aim was to simulate the instrumental spectrum of the detector used in the experiment.

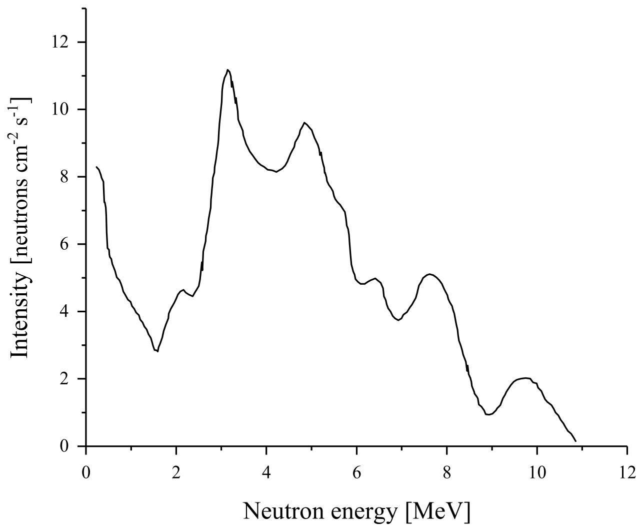

Fig. 3. Digitized neutron energy spectrum of the ^{241}Am–Be source measured in [13].

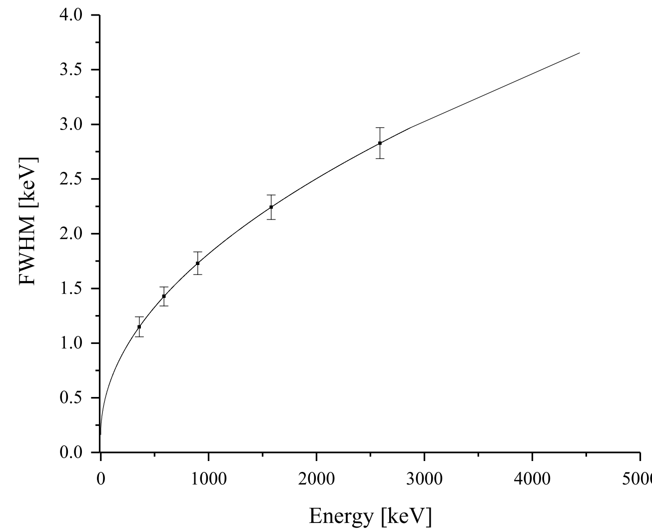

Fig. 4. Energy resolution of the Ge detector used in the experiment.

Real conditions were implemented into the Monte Carlo simulation. The simulated source matches the shape and dimensions of the real source and it emits particles isotropically.

The precise geometry setup was coded including individual material compositions. Special attention was paid to impurity in different materials. Investigation of impurities was carried out and every known material impurity was incorporated into simulation. The physics list SHIELDING, developed for neutron penetration studies and ion–ion collisions, was used in the simulations. It contains the best selection of electromagnetic and hadronic physical processes required to solve shielding problems including low background experiments. During simulation, every particle and process were tracked including particle's kinematics. The deposited energy was recorded each time a particle hit the detector.

3. Results and discussion

A detailed analysis of the experimental spectrum was carried out. To make the peaks more visible, the spectrum was split into three parts with energy ranges 0–1 MeV (Fig. 5), 1–2 MeV (Fig. 6) and 2–3 MeV (Fig. 7). Almost all peaks in the spectra were identified and explained. A typical feature of neutron interactions with a Ge detector are triangular γ-ray peaks. When a germanium detector is exposed to neutrons at energies of 1 MeV or more, triangular peaks may result from summation of the recoil energy of a Ge nucleus deposited within the detector itself and the energy of a photon emitted during de-excitation of the nucleus previously excited during inelastic scattering [4]. In the experiment, such peaks were observed at the energies of 68.80 keV, 562.93 keV, 595.84 keV, 689.60 keV, 834.01 keV, 1039.51 keV, 1108.41 keV, 1204.20 keV and 1463.75 keV.

The 68.80 keV peak corresponds to the reaction ^{73}Ge(n, n′γ)^{73}Ge* (the symbol "*" indicates excited states for very short living radionuclides with half-lives less than 1 ms). The 562.93 keV and 1108.41 keV peaks originate from inelastic scattering of neutrons on ^{76}Ge while the 689.60 keV and 834.01 keV peaks are results of the reaction ^{72}Ge(n, n′γ)^{72}Ge*. The peaks at energies of 595.84 keV, 1204.20 keV and 1463.75 keV originate from inelastic scattering of neutrons on ^{74}Ge. And finally, the 1039.51 keV peak corresponds to the reaction ^{70}Ge(n, n′γ)^{70}Ge*.

In the case of the 691.43 keV peak (Fig. 5), the induction mechanism is slightly different. The excited nucleus of ^{72}Ge de-excites by an E0 transition, which is an internal conversion process for this nuclide: ^{72}Ge(n,

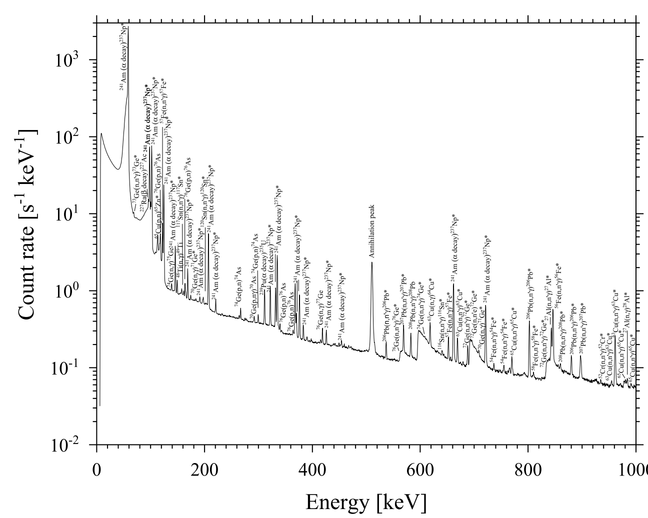

Fig. 5. Experimental γ-spectrum of neutron and γ-ray interactions with Ge detector for energy range of 0–1 MeV.

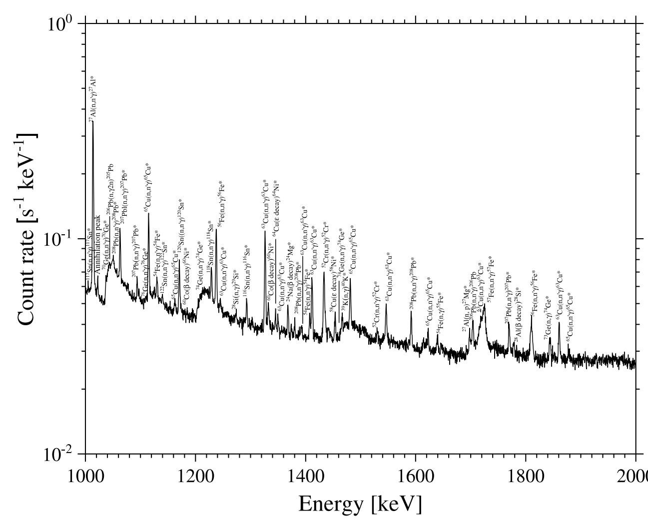

Fig. 6. Experimental γ-spectrum of neutron and γ-ray interactions with Ge detector for energy range of 1–2 MeV.

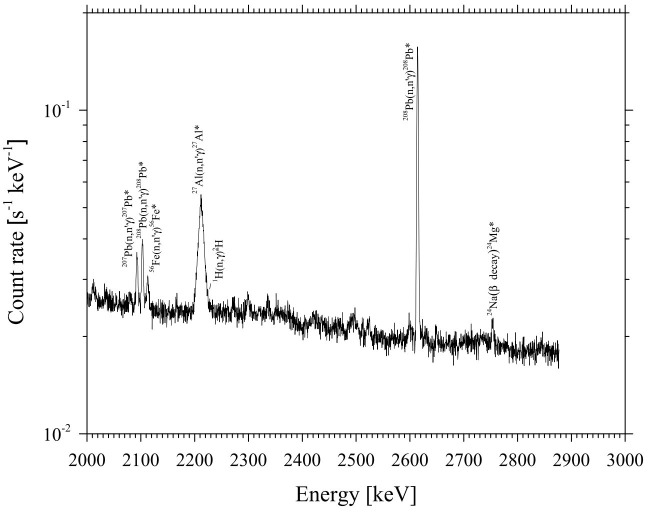

Fig. 7. Experimental γ-spectrum of neutron and γ-ray interactions with Ge detector for energy range of 2–3 MeV.

n′e)^{72}Ge*. The total detectable energy of ^{72}Ge includes the energy from the X-ray and it is summed with the recoil energy of the ^{72}Ge nucleus to form a triangular shape [15]. A small triangular peak at the energy of 608.35 keV (Fig. 5) originates from the cascade of 1204.20 keV level in ^{74}Ge, if the following 595.84 keV γ-ray escapes from the detector [4]. The peak is visible in the upper part of the ^{74}Ge triangular peak at energy of 595.84 keV. The shapes of the triangular peaks are sharp at lower energies but lose their sharpness with increasing energy. The reason is difference between angular distributions of the neutron scattering on the separate Ge isotopes [4].

A large number of other peaks were observed in the spectra which are caused by neutron interactions with all materials in the setup, and particularly with impurities. Most of the peaks, which clearly dominate in the spectra are from lead and copper, the most abundant materials around the Ge crystal. They originate from inelastic scattering of neutrons on copper and lead nuclei. The ^{208}Pb peak at the energy of 2614.51 keV is a result of the reaction ^{208}Pb(n, n′γ)^{208}Pb*, and the peaks at the energies of 2103.51 keV and 1592.51 keV are single and double escape peaks, respectively. Lead-208 is one of lead stable isotopes with the highest natural abundance of 52.4%. Other stable isotopes of Pb include ^{204}Pb, ^{206}Pb and ^{207}Pb with abundances of 1.4%, 24.1% and 22.1%, respectively. Peaks from ^{208}Pb are also visible at energies of 583.18 keV, 860.56 keV, 1050.90 keV and 1380.89 keV. Lead-207 peaks are visible in the spectra at the energies of 569.70 keV, 897.77 keV, 1063.66 keV, 1094.70 keV, 1770.23 keV and 2092.78 keV. Gamma-lines of ^{206}Pb are visible at energies of 537.47 keV, 803.06 keV, 880.98 keV and 1704.45 keV. The 1043.75 keV peak is induced by the reaction ^{206}Pb(n, 2nγ)^{205}Pb, a different reaction type.

Copper has two naturally occurring isotopes,^{63}Cu and ^{65}Cu, with abundances of 69.15% and 30.85%, respectively. Gamma lines of ^{63}Cu were observed at the energies of 669.62 keV, 955.0 keV, 962.06 keV, 1245.20 keV, 1327.03 keV, 1350.10 keV, 1392.55 keV, 1412.08 keV, 1547.04 keV, 1716.80 keV and 1861.30 keV. The ^{63}Cu peak at 1716.80 keV has an interfering 1725.09 keV γ-ray originating in inelastic scattering on ^{57}Fe. The isotope ^{65}Cu gives rise to peaks at the energies of 770.60 keV, 978.80 keV, 990.0 keV, 1115.55 keV, 1162.60 keV, 1481.84 keV, 1623.42 keV and 1879.0 keV. The γ-line at the energy of 617.43 keV originates from the neutron capture on ^{63}Cu, which results in a compound nucleus of ^{64}Cu. The copper γ-lines come from the copper crystal holder and the copper cladding of the shield. The lead γ-lines originate from the lead part of the shield, which is the largest one.

The aluminium lines at the energies of 843.76 keV, 1014.52 keV and 2212.01 keV are from the first, the second and the third exited states of ^{27}Al respectively. They are induced by inelastic scattering of neutrons on ^{27}Al nuclei. The peak at 2212.01 keV is broad because of the Doppler effect: γ-rays are emitted while the excited nucleus is still moving after receiving a kick from the impinging neutron [16]. The 983.02 keV peak of ^{28}Al originates from the neutron capture on ^{27}Al. Almost all aluminium γ-rays are from the aluminium shell of the source and from the detector cryostat. Small amounts of aluminium are also present in the Ge crystal and in the iron absorbers as impurity.

A small peak at the energy of 2224.56 keV corresponding to the neutron capture on hydrogen was also observed but it is in the upper edge of a broad peak from aluminium at 2212.01 keV (Fig. 7). The ^{27}Al γ-rays interfere with ^{2}H γ-rays strongly. Hydrogen is present in plastic parts of the setup.

The γ-rays from inelastic scattering of neutrons on iron nuclei are present in the spectra, too. Iron has four stable isotopes, ^{54}Fe, ^{56}Fe, ^{57}Fe and ^{58}Fe, with abundance of 5.85%, 91.75%, 2.12% and 0.28%, respectively. Peaks from ^{57}Fe are visible at the energies of 122.06 keV, 650.40 keV and 1725.09 keV. Peaks from ^{54}Fe are observable at the energies of 736.40 keV, 756.60 keV, 1129.90 keV and 1408.10 keV. Peaks from ^{56}Fe are present in the spectra at the energies of 846.76 keV, 1238.27 keV, 1810.76 keV and 2113.14 keV. There is only one line from ^{58}Fe present: 810.76 keV. The peak of ^{55}Fe at the energy 1640.40 keV originates from the neutron capture on ^{54}Fe. The sources of the iron peaks are mostly the iron in the ^{241}Am–Be source encapsulation and iron in the absorbers.

The γ-rays from inelastic scattering of neutrons on tin nuclei are also visible in the spectra. Lines of ^{117}Sn are visible at the energies of 158.56 keV, 1004.51 keV, lines of ^{120}Sn at the energies of 197.37 keV, 1171.25 keV, lines of ^{116}Sn at the energies of 641.10 keV and 1293.56 keV, line of ^{122}Sn at the energy of 1140.52 keV and a line of ^{118}Sn at the energy of 1229.68 keV. The sources of tin peaks are iron absorbers that are tin-plated and the tin layer of the shield.

Although various impurities are present in small amounts in the setup, they may be important thanks to large neutron cross-sections for certain isotopes. A peak of ^{49}Ti at the energy of 149.56 keV originates from the neutron capture on ^{48}Ti that is present in stainless steel as impurity so as Cr and Si. The peaks of ^{52}Cr isotope induced by inelastic scattering of neutrons on chromium nuclei are visible at the energies of 935.54 keV, 1434.07 keV and 1530.67 keV. There are two peaks from Si: a 1273.36 keV peak of ^{29}Si and a 1778.97 keV peak of ^{28}Si. Beta decay of the activation product ^{28}Al is also contributing to the latter peak through its daughter ^{28}Si.

The peaks at the energies of 2754.01 keV and 1368.63 keV come from the β decay of ^{24}Na produced in the ^{27}Al(n, α)^{24}Na reaction in aluminium. A line of ^{27}Mg is visible in the spectrum as well, at the energy of 1698.46 keV. It originates from the ^{27}Al(n, p)^{27}Mg reaction, while magnesium subsequently decayed by β decay to ^{27}Al.

The ^{40}K peak (1466.11 keV) is the special one. It results from de-excitation of ^{40}K produced by neutron capture on ^{39}K (abundance of 93.258%). It should not be confused with the 1460.80 keV peak (frequently observed in background) produced after the electron-capture decay of ^{40}K that actually corresponds to de-excitation of the daughter nucleus ^{40}Ar. The other potassium isotopes (^{40}K and ^{41}K) have too small abundances so the neutron reaction products were not visible. Potassium is present in the material surrounding the detector, but also in the circular iron absorbers as impurity (0.026%). Solutions of potassium-stannate and potassium-hydroxide were also used as plating bath for alkali tin plating of metals [17].

Many peaks are results of proton and electron interactions with materials of the setup, especially with Ge crystal, copper and stainless-steel parts. Protons and electrons were produced by β-decays of free neutrons, and protons were also produced in (n, p) reactions. ^{58}Cu (line 848.60 keV) was produced from ^{58}Ni (abundance of 68.077%, present as impurity in stainless steel material) by (p, n) reaction, which subsequently decayed by electron capture back to ^{58}Ni (line 1454.28 keV). ^{64}Cu (line 617.43 keV) was produced by neutron capture on ^{63}Cu (abundance of 69.15%). ^{65}Zn (line 115.09 keV) was produced in (p, n) reaction on ^{65}Cu (abundance of 30.85%). ^{64}Ni (line 1345.84 keV) was produced in electron capture decay of ^{64}Cu.

^{74}As at energies of 267.43 keV and 299.97 keV, ^{76}As at energies of 139.68 keV, 165.05 keV, 339.33 keV and 363.91 keV were produced in (p, n) reactions on ^{74}Ge and ^{76}Ge nuclei. Peaks resulting from the neutron capture on Ge isotopes were detected, too. Namely, at 138.9 keV from ^{74}Ge(n, γ)^{75}Ge, at 418.50 keV from ^{76}Ge(n, γ)^{77}Ge, at 174.96 keV and 708.19 keV from ^{70}Ge(n, γ)^{71}Ge, and at 1844.62 keV from ^{73}Ge(n, γ)^{74}Ge. ^{70}As at energy of 293.66 keV originated from (p, nγ) reaction on ^{70}Ge. The well-known ^{60}Co peaks at 1173.23 keV and 1332.51 keV represents excited levels in stable ^{60}Ni (abundance of 26.223%) after inelastic scattering of neutrons. Another source could be the β-decay of ^{60}Co produced by activation of iron absorbers.

The peak with highest count rate in the spectrum at the energy of 58.54 keV is the γ-line of ^{237}Np that is a decay product of ^{241}Am. The other observed lines have energies of 98.97 keV, 102.98 keV, 125.3 keV, 146.55 keV, 169.56 keV, 191.96 keV, 208.10 keV, 221.80 keV, 322.52 keV, 332.35 keV, 335.37 keV, 368.62 keV, 370.94 keV, 376.65 keV, 383.81 keV, 426.47 keV, 454.66 keV, 662.40 keV and 722.01 keV.

The peak at the energy of 96.80 keV (^{227}Ac) is coming from β-decay of ^{227}Ra. The peak at the energy of 311.78 keV (^{235}U) originates from α-decay of ^{239}Pu. ^{227}Ra and ^{239}Pu are radioactive contaminants of the ^{241}Am–Be source. ^{227}Ra is produced by the source neutrons captured on ^{226}Ra that is present in the neutron source as an impurity.

The peaks at the energies of 511 keV and 1022 keV come from annihilation of electron–positron pairs generated by photon interactions with materials of the setup.

Presence of copper and lead influences the γ-spectrum strongly. Interactions of neutrons with these materials produce many γ-lines visible in the spectrum, which can hide or imitate searched signals. This is an unwanted effect, especially in experiments looking for rare nuclear processes. For example γ-rays resulting from neutron inelastic scattering or neutron capture reactions may imitate signatures of the neutrinoless $\beta\beta$ decay [18]. Possible replacement of copper and lead as shielding materials in underground experiments would require, however, further investigations.

Aluminium has only a few strong γ-lines in the spectrum, and it is certainly a significant background component. To avoid its contribution is, however, very difficult, because aluminium is the most commonly used material for cryostats and entrance windows. Nevertheless, the problem can be solved by elaboration of appropriate event-rejection strategy.

Similarly, γ-lines from tin parts of the setup are important potential sources of background. However, tin layers are usually not present in shields of Ge detectors located deeply underground. As it was shown previously, descending-Z shields consisting of lead, tin and copper are superior as far as the muon background is concerned [19]. Once it is suppressed, passively and/or actively, more materials remain for consideration.

To minimize the background induced by neutron interactions with impurities in the materials, it is necessary to use ultra-pure materials for experimental setups, and to know the identity and the amount of the residual elements.

In shallow as well as in deep underground laboratories fast neutrons are always present. They are produced by cosmic-ray interactions generating hadron showers as well as by capture of negative muons, predominantly on heavy nuclei like lead. Hence, inelastic scattering will always contribute to the background of Ge detectors in the energy region of interest manifesting itself by Ge peaks observed experimentally. If the spectrum statistics is sufficient to recognize such peaks, the contribution of neutrons to the total background can be unfolded. However, validated Monte Carlo simulations should be always carried out for estimation of the neutron background component.

4. Comparison of experimental and simulated γ-spectra

The experimental and simulated γ-spectra are shown in Fig. 8. The experimental spectrum was compared with the GEANT4 simulation of neutron and γ-ray interactions with the detector and the shield. The simulated spectrum reproduces the main features of the measured spectrum fairly well considering the complexity of the interactions. Integral count rates were compared for the experimental and the simulated spectra for the energy region from 250 keV to 2880 keV. This energy range was chosen due to a difference between experimental and simulated data for a lower continuum below 250 keV (explained below) and the end of the measured spectrum at 2880 keV. The integral count rate measured in the experiment (210 ± 2 s^{-1}) was in reasonable agreement with computed (197 ± 9 s^{-1}) result.

All peaks in the experimental γ-spectrum are clearly visible in the simulation, except peaks from the β decay of ^{227}Ra and α decay of ^{239}Pu resulting from contamination of the source, and γ-lines of ^{237}Np emitted after the α decay of ^{241}Am. The γ-emission of ^{241}Am is represented in the simulated spectrum only by the strongest γ-line at the energy of 59.54 keV and no other weaker γ-lines resulting from the ^{241}Am decay was generated in the simulation. The beginning of the simulated spectrum up to energy of 250 keV has a different shape than the beginning of the experimental spectrum, which may be due to a lower γ-ray intensity of the simulated ^{241}Am–Be source. The γ-ray intensity of neutron source is important information as well as intensity of neutrons. Intensity of γ-rays was calculated on the base of known neutron flux of ^{241}Am–Be source and γ-emission of ^{241}Am isotope, determined from the activity of the neutron source. The intensity of 4.44 MeV γ-rays was calculated as 75% of the neutron intensity [20]. Nevertheless, the real γ-ray intensity of the neutron source was evidently higher.

The triangular Ge peaks in the simulated γ-spectrum are lower and less sharp than in the measured spectrum, which is given by the physics implemented in GEANT4. The software is not yet capable to simulate appropriately Ge peaks at lower neutron energies, while for higher neutron energies, above 10 MeV, it simulates well. The average neutron energy in the simulation was 4.2 MeV.

^{27}Al peak (2982.0 keV) resulting from inelastic scattering of neutrons on aluminium nuclei is visible in the simulated spectra. This peak is not present in the experimental spectrum that extends only till 2880 keV. Also, a peak at the energy of 477.61 keV coming from ^{10}B(n, α)^{7}Li reaction is not visible in the measured spectrum. This peak is hidden in the continuum of photons generated during the experiment, but not simulated. The ^{241}Am–Be source emits much more γ-rays than neutrons (5800:1 for 370 MBq source) and the region till 500 keV is significantly affected by γ-rays from ^{241}Am. Also, the amount of boron in the setup is too small, so the thermal neutron capture by boron and subsequent emission of α-particle and 477.61 keV γ-ray is not visible in the experimental spectrum.

New simulation was carried out with the aim to achieve better agreement between the experiment and the simulation, and to assess the impact of further γ-rays of ^{241}Am on the shape of simulated spectrum. Instead of Gaussian energy distribution of ^{241}Am γ-rays, ^{241}Am ion was coded as input parameter for particle gun including complete decay process. Both spectra are visible separately in Fig. 9. The comparison of the experiment with the simulation shows that inclusion of ^{241}Am ion into simulation increased the γ-ray intensity of the simulated ^{241}Am–Be source, and additional ^{237}Np peaks from ^{241}Am decay are visible in the simulated spectrum. Therefore the shape of the beginning of the simulated spectrum was lifted up. However, there is still a little difference in the region till 115 keV, especially between the measured and simulated photopeak of ^{241}Am. The measured photopeak is about one order of magnitude higher than the simulated one. This can be probably explained by non-exact inputs for the ^{241}Am source implemented in GEANT4. The integral count rate measured in the energy region from 115 keV to 2880 keV (378 ± 3 s^{-1}) was in reasonable agreement with

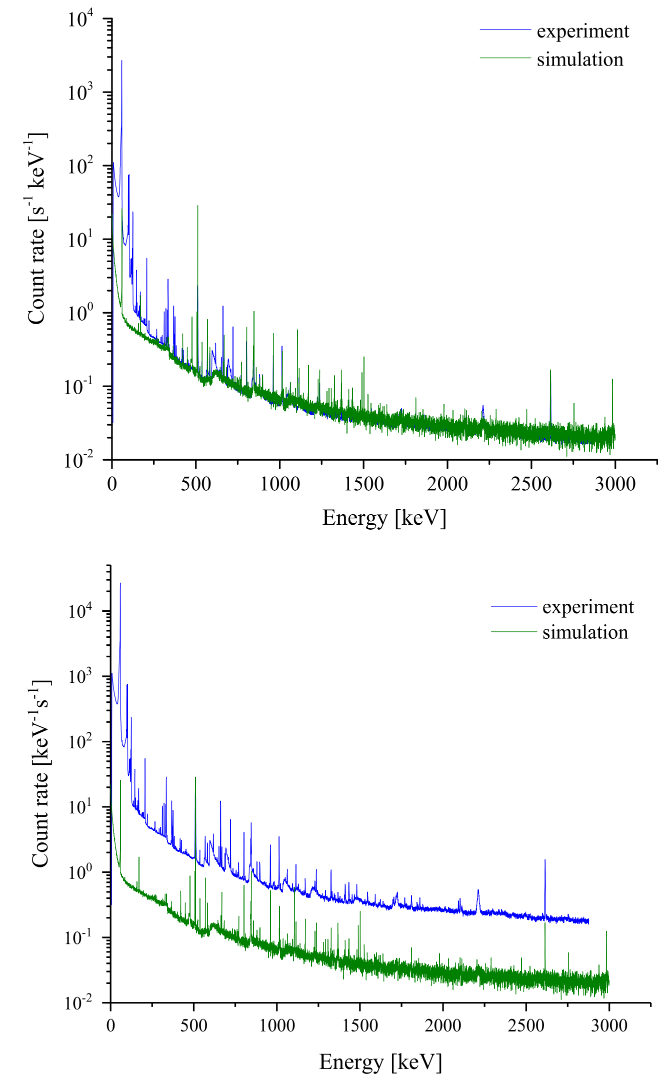

Fig. 8. Comparison of experimental and simulated γ-spectra (the experimental spectrum shown in the bottom figure has been multiplied by 10 for better visibility). The simulation was carried out with Gaussian energy distribution of ^{241}Am γ-rays coded in GEANT4.

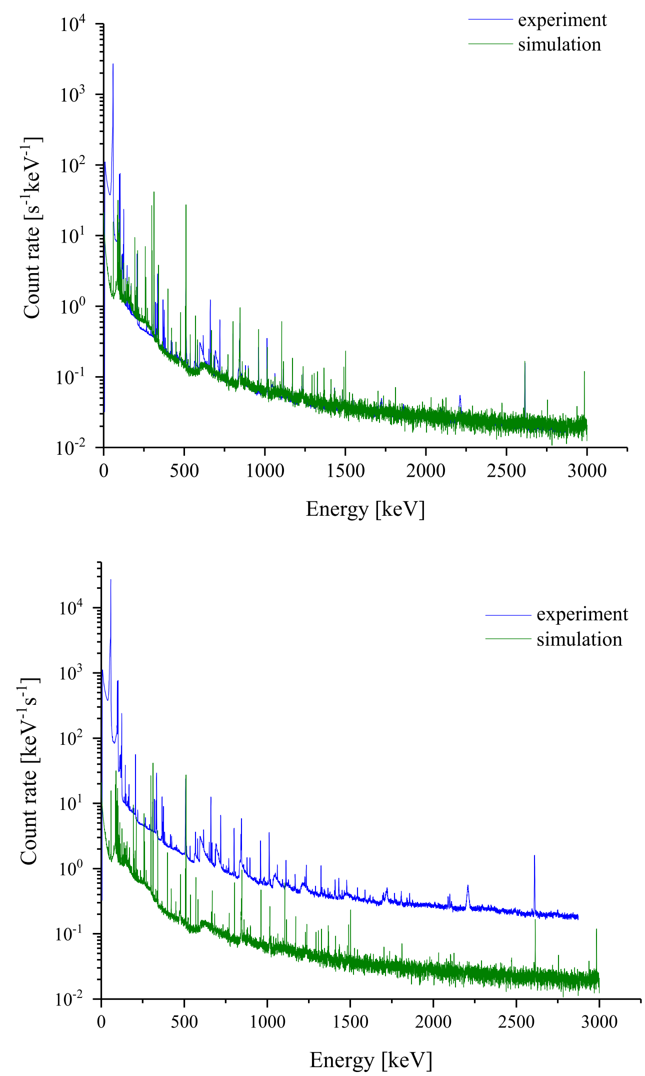

Fig. 9. Comparison of experimental and simulated γ-spectra (the experimental spectrum shown in the bottom figure has been multiplied by 10 for better visibility). The simulation was carried out using ^{241}Am ion in GEANT4 instead of Gaussian energy distribution as a source of ^{241}Am γ-rays.

calculated (369 ± 11 s^{-1}) one. All measured and calculated results are listed in the accompanying Table 2 to this paper.

5. Conclusions

Investigations of interactions of neutrons (produced in the ^{241}Am–Be source) with Ge detector placed in low-level shielding were carried out experimentally and compared with Monte Carlo simulation using GEANT4 tool. Precise geometry of the setup was coded including individual material impurities. Reactions of elastic and inelastic scattering of fast neutrons were observed, as well as their capture by Ge and other nuclei present in the set up. Typical triangular shape γ-peaks of ^{70}Ge, ^{72}Ge, ^{73}Ge, ^{74}Ge and ^{76}Ge induced by inelastic scattering of neutrons were detected. A large number of other peaks induced by neutron interactions with all materials in the setup (including impurities) were observed. Gamma-lines resulting from neutron interactions with lead and copper parts of the setup (e.g. the peak at 2614.51 keV originating from the reaction of ^{208}Pb(n, n′γ)^{208}Pb*), dominated in the spectra. The peak of ^{40}K (1466.11 keV) was detected only as an excited state resulting from neutron capture by ^{39}K. Impurities in materials are important targets for neutron interactions and their inclusion into simulation provide a better agreement with the experiment, also important for deep underground installations. Simulated background γ-spectra were in good agreement with the experimental ones, except for a lower-energy range below 250 keV.

This work provides a thorough analysis of peaks observed in γ-spectra measured by Ge spectrometers exposed to fast neutrons, and demonstrates GEANT4 as a useful tool for simulating neutron-induced background of Ge spectrometers.

Acknowledgements

The authors are thankful to CERN for providing Ph.D. fellowship to Miloslava Baginova. Special thanks to Fabrice Malacrida for his help with the neutron source and the experiment. Support provided by the Slovak Research and Development Agency (project no. 15-0576) is highly acknowledged.

Table 2
Table of measured and simulated count rates.

Energy peaks [keV]	Nuclides and Reactions	Count rates [s^{-1}]	
		Experiment	Simulation (^{241}Am ion in GEANT4)
115–2880	Continuum	378 ± 3	369 ± 11
59.54	^{241}Am (α decay)^{237}Np*	2450 ± 30	5.42 ± 0.21
68.80	^{73}Ge(n, n'γ)^{73}Ge*	0.82 ± 0.06	0.06 ± 0.06
96.80	^{227}Ra(β decay)^{227}Ac	1.66 ± 0.05	–
98.97	^{241}Am (α decay)^{237}Np*	66.55 ± 0.80	7.32 ± 0.31
102.98	^{241}Am (α decay)^{237}Np*	73.1 ± 0.8	1.67 ± 0.17
115.09	^{65}Cu(p, n)^{65}Zn*	3.11 ± 0.05	2.39 ± 0.14
118.68	^{76}Ge(p, n)^{76}As	2.33 ± 0.04	0.12 ± 0.08
122.06	^{57}Fe(n, n'γ)^{57}Fe*	4.82 ± 0.03	0.13 ± 0.08
125.30	^{241}Am (α decay)^{237}Np*	23.9 ± 0.1	1.11 ± 0.06
139.68	^{74}Ge(n, γ)^{75}Ge	0.29 ± 0.03	0.69 ± 0.18
146.55	^{241}Am (α decay)^{237}Np*	3.28 ± 0.03	0.54 ± 0.12
149.56	^{48}Ti(n, γ)^{49}Ti	0.54 ± 0.03	0.10 ± 0.07
158.56	^{117}Sn(n, n'γ)^{117}Sn*	0.19 ± 0.02	0.11 ± 0.08
165.05	^{76}Ge(p,n)^{76}As	0.48 ± 0.03	0.17 ± 0.08
169.56	^{241}Am (α decay)^{237}Np*	1.37 ± 0.03	1.31 ± 0.11
174.96	^{70}Ge(n, γ)^{71}Ge*	0.15 ± 0.02	0.05 ± 0.06
191.96	^{241}Am (α decay)^{237}Np*	0.19 ± 0.03	3.28 ± 0.16
197.37	^{120}Sn(n, n'γ)^{120}Sn*	0.72 ± 0.02	0.30 ± 0.05
208.01	^{241}Am (α decay)^{237}Np*	6.22 ± 0.08	2.10 ± 0.11
221.80	^{241}Am (α decay)^{237}Np*	0.34 ± 0.02	0.08 ± 0.08
267.43	^{74}Ge(p, n)^{74}As	0.20 ± 0.02	0.03 ± 0.05
293.66	^{70}Ge(p, nγ)^{70}As	0.10 ± 0.02	0.03 ± 0.05
299.97	^{74}Ge(p, n)^{74}As	0.17 ± 0.02	2.10 ± 0.10
311.78	^{239}Pu(α decay)^{235}U	0.92 ± 0.02	–
322.52	^{241}Am (α decay)^{237}Np*	1.06 ± 0.02	0.04 ± 0.04
332.35	^{241}Am (α decay)^{237}Np*	0.94 ± 0.02	0.03 ± 0.03
335.37	^{241}Am (α decay)^{237}Np*	3.26 ± 0.02	0.12 ± 0.05
339.33	^{76}Ge(p, n)^{76}As	0.10 ± 0.01	1.30 ± 0.05
363.91	^{76}Ge(p, n)^{76}As	0.04 ± 0.02	0.02 ± 0.02
368.62	^{241}Am (α decay)^{237}Np*	1.21 ± 0.02	0.01 ± 0.02
370.94	^{241}Am (α decay)^{237}Np*	0.17 ± 0.02	0.04 ± 0.04
376.65	^{241}Am (α decay)^{237}Np*	0.93 ± 0.02	0.05 ± 0.03
383.81	^{241}Am (α decay)^{237}Np*	0.19 ± 0.02	0.05 ± 0.04
418.50	^{76}Ge(n, γ)^{77}Ge	0.16 ± 0.01	0.73 ± 0.07
426.47	^{241}Am (α decay)^{237}Np*	0.15 ± 0.01	0.02 ± 0.03
454.66	^{241}Am (α decay)^{237}Np*	0.07 ± 0.02	0.02 ± 0.01
511	Annihilation	6.11 ± 0.08	9.99 ± 0.50
537.47	^{206}Pb(n, n'γ)^{206}Pb*	0.13 ± 0.02	0.11 ± 0.03
562.93	^{76}Ge(n, n'γ)^{76}Ge*	0.07 ± 0.02	0.02 ± 0.03
569.70	^{207}Pb(n, n'γ)^{207}Pb*	0.31 ± 0.02	0.29 ± 0.03
583.18	^{208}Pb(n, n'γ)^{208}Pb*	0.22 ± 0.02	0.18 ± 0.03
595.84	^{74}Ge(n, n'γ)^{74}Ge*	0.20 ± 0.02	0.02 ± 0.03
608.35	^{74}Ge(n, n'γ)^{74}Ge*	0.02 ± 0.02	0.03 ± 0.03
617.43	^{63}Cu(n, γ)^{64}Cu*	0.31 ± 0.02	0.04 ± 0.03
641.10	^{116}Sn(n, n'γ)^{116}Sn*	0.04 ± 0.02	0.02 ± 0.01
650.40	^{57}Fe(n, n'γ)^{57}Fe*	0.18 ± 0.01	0.01 ± 0.02
662.40	^{241}Am (α decay)^{237}Np*	1.89 ± 0.02	0.10 ± 0.04
669.62	^{63}Cu(n ,n'γ)^{63}Cu*	0.23 ± 0.02	0.18 ± 0.04
689.60	^{72}Ge(n, n'γ)^{72}Ge*	0.10 ± 0.01	0.01 ± 0.02
691.43	^{72}Ge(n, n'e)^{72}Ge*	0.34 ± 0.02	0.04 ± 0.03
708.19	^{70}Ge(n, γ)^{71}Ge*	0.04 ± 0.01	0.02 ± 0.03
722.01	^{241}Am (α decay)^{237}Np*	0.91 ± 0.02	0.06 ± 0.05
736.40	^{54}Fe(n, n'γ)^{54}Fe*	0.05 ± 0.01	0.04 ± 0.03
756.60	^{54}Fe(n, n'γ)^{54}Fe*	0.03 ± 0.01	0.02 ± 0.02
770.60	^{65}Cu(n, n'γ)^{65}Cu*	0.10 ± 0.01	0.10 ± 0.03
803.06	^{206}Pb(n, n'γ)^{206}Pb*	0.58 ± 0.02	0.30 ± 0.03
810.76	^{58}Fe(n, n'γ)^{58}Fe*	0.02 ± 0.01	0.01 ± 0.01
834.01	^{72}Ge(n, n'γ)^{72}Ge*	0.15 ± 0.02	0.03 ± 0.03
843.76	^{27}Al(n, n'γ)^{27}Al*	0.23 ± 0.01	0.57 ± 0.04
846.76	^{56}Fe(n, n'γ)^{56}Fe*	0.66 ± 0.01	0.78 ± 0.04
860.56	^{208}Pb(n, n'γ)^{208}Pb*	0.03 ± 0.02	0.61 ± 0.04
880.98	^{206}Pb(n, n'γ)^{206}Pb*	0.14 ± 0.01	0.50 ± 0.03
897.77	^{207}Pb(n, n'γ)^{207}Pb*	0.18 ± 0.01	0.08 ± 0.03
935.54	^{52}Cr(n, n'γ)^{52}Cr*	0.01 ± 0.01	0.02 ± 0.02
955.0	^{63}Cu(n, n'γ)^{63}Cu*	0.03 ± 0.01	0.04 ± 0.03
962.06	^{63}Cu(n, n'γ)^{63}Cu*	0.40 ± 0.01	0.21 ± 0.03
978.80	^{65}Cu(n, n'γ)^{65}Cu*	0.02 ± 0.01	0.01 ± 0.01
983.02	^{27}Al(n, γ)^{28}Al*	0.03 ± 0.01	0.02 ± 0.02
990.0	^{63}Cu(n, n'γ)^{63}Cu*	0.02 ± 0.01	0.02 ± 0.01
1004.51	^{117}Sn(n, n'γ)^{117}Sn*	0.01 ± 0.01	0.03 ± 0.03

(*continued on next page*)

Table 2 (*continued*)

Energy peaks [keV]	Nuclides and Reactions	Count rates [s^{-1}]	
		Experiment	Simulation (^{241}Am ion in GEANT4)
1014.52	^{27}Al(n, n'γ)^{27}Al*	0.59 ± 0.01	0.08 ± 0.02
1022	Annihilation	0.02 ± 0.01	0.02 ± 0.01
1039.51	^{70}Ge(n, n'γ)^{70}Ge*	0.03 ± 0.02	0.03 ± 0.02
1043.75	^{206}Pb(n, γ2n)^{205}Pb*	0.01 ± 0.01	0.01 ± 0.02
1050.90	^{208}Pb(n, n'γ)^{208}Pb*	0.02 ± 0.01	0.02 ± 0.02
1063.66	^{207}Pb(n, n'γ)^{207}Pb*	0.09 ± 0.01	0.04 ± 0.03
1094.70	^{207}Pb(n, n'γ)^{207}Pb*	0.02 ± 0.01	0.02 ± 0.01
1108.41	^{76}Ge(n, n'γ)^{76}Ge*	0.01 ± 0.01	0.27 ± 0.02
1115.55	^{65}Cu(n, n'γ)^{65}Cu*	0.16 ± 0.01	0.10 ± 0.01
1129.90	^{54}Fe(n, n'γ)^{54}Fe*	0.03 ± 0.01	0.01 ± 0.01
1140.52	^{122}Sn(n, n'γ)^{122}Sn*	0.01 ± 0.01	0.01 ± 0.01
1162.60	^{65}Cu(n, n'γ)^{65}Cu*	0.02 ± 0.01	0.01 ± 0.02
1171.25	^{120}Sn(n, n'γ)^{120}Sn*	0.07 ± 0.01	0.06 ± 0.01
1173.23	^{60}Co(β decay)^{60}Ni*	0.01 ± 0.01	0.01 ± 0.02
1204.20	^{74}Ge(n, n'γ)^{74}Ge*	0.01 ± 0.01	0.01 ± 0.01
1229.68	^{118}Sn(n, n'γ)^{118}Sn*	0.05 ± 0.01	0.03 ± 0.02
1238.27	^{56}Fe(n, n'γ)^{56}Fe*	0.12 ± 0.01	0.04 ± 0.01
1245.20	^{63}Cu(n, n'γ)^{63}Cu*	0.01 ± 0.01	0.02 ± 0.02
1273.36	^{28}Si(n, γ)^{29}Si*	0.02 ± 0.01	0.01 ± 0.01
1293.56	^{116}Sn(n, n'γ)^{116}Sn*	0.03 ± 0.01	0.04 ± 0.02
1327.03	^{63}Cu(n, n'γ)^{63}Cu*	0.14 ± 0.01	0.07 ± 0.03
1332.51	^{60}Co(β decay)^{60}Ni*	0.02 ± 0.01	0.01 ± 0.01
1345.84	^{64}Cu(ε decay)^{64}Ni*	0.01 ± 0.01	0.01 ± 0.01
1350.10	^{63}Cu(n, n'γ)^{63}Cu*	0.01 ± 0.01	0.01 ± 0.01
1368.63	^{24}Na(β decay)^{24}Mg*	0.03 ± 0.01	0.04 ± 0.02
1380.89	^{208}Pb(n, n'γ)^{208}Pb*	0.01 ± 0.01	0.01 ± 0.01
1392.55	^{63}Cu(n, n'γ)^{63}Cu*	0.01 ± 0.01	0.03 ± 0.02
1408.10	^{54}Fe(n, n'γ)^{54}Fe*	0.02 ± 0.01	0.02 ± 0.01
1412.08	^{63}Cu(n, n'γ)^{63}Cu*	0.07 ± 0.01	0.03 ± 0.01
1434.07	^{52}Cr(n, n'γ)^{52}Cr*	0.10 ± 0.01	0.02 ± 0.01
1454.28	^{58}Cu(ε decay)^{58}Ni*	0.03 ± 0.01	0.01 ± 0.01
1463.75	^{74}Ge(n, n'γ)^{74}Ge*	0.02 ± 0.02	0.02 ± 0.01
1466.11	^{39}K(n, γ)^{40}K*	0.01 ± 0.01	0.02 ± 0.01
1481.84	^{65}Cu(n, n'γ)^{65}Cu*	0.06 ± 0.01	0.02 ± 0.01
1530.67	^{52}Cr(n, n'γ)^{52}Cr*	0.01 ± 0.01	0.01 ± 0.01
1547.04	^{63}Cu(n, n'γ)^{63}Cu*	0.03 ± 0.01	0.02 ± 0.01
1592.51	Single escape peak of 2614.51 keV	0.03 ± 0.01	0.02 ± 0.01
1623.42	^{65}Cu(n, n'γ)^{65}Cu*	0.01 ± 0.01	0.01 ± 0.01
1640.40	^{54}Fe(n, γ)^{55}Fe*	0.01 ± 0.01	0.02 ± 0.01
1698.46	^{27}Al(β decay)^{27}Mg*	0.01 ± 0.01	0.01 ± 0.01
1704.45	^{206}Pb(n, n'γ)^{206}Pb*	0.03 ± 0.01	0.03 ± 0.01
1716.80	^{63}Cu(n, n'γ)^{63}Cu*	0.01 ± 0.01	0.02 ± 0.02
1725.09	^{57}Fe(n, n'γ)^{57}Fe*	0.02 ± 0.01	0.01 ± 0.01
1770.23	^{207}Pb(n, n'γ)^{207}Pb*	0.03 ± 0.01	0.02 ± 0.01
1778.97	^{28}Al(β decay)^{28}Si*	0.01 ± 0.01	0.02 ± 0.01
1810.76	^{56}Fe(n, n'γ)^{56}Fe*	0.04 ± 0.01	0.03 ± 0.02
1844.62	^{73}Ge(n, γ)^{74}Ge*	0.03 ± 0.01	0.03 ± 0.02
1861.30	^{63}Cu(n, n'γ)^{63}Cu*	0.03 ± 0.01	0.01 ± 0.01
1879.0	^{65}Cu(n, n'γ)^{65}Cu*	0.01 ± 0.01	0.02 ± 0.02
2092.78	^{207}Pb(n, n'γ)^{207}Pb*	0.04 ± 0.01	0.02 ± 0.01
2103.51	Double escape peak of 2614.51 keV	0.05 ± 0.01	0.02 ± 0.01
2113.14	^{56}Fe(n, n'γ)^{56}Fe*	0.01 ± 0.01	0.01 ± 0.01
2212.01	^{27}Al(n, n'γ)^{27}Al*	0.07 ± 0.02	0.03 ± 0.01
2224.56	^{1}H(n, γ)^{2}H	0.01 ± 0.01	0.01 ± 0.01
2614.51	^{208}Pb(n, n'γ)^{208}Pb*	0.44 ± 0.01	0.19 ± 0.02
2754.01	^{24}Na(β decay)^{24}Mg*	0.01 ± 0.01	0.01 ± 0.01

References

[1] R. Breier, P. Povinec, Simulation of background of low-level gamma-ray spectrometers using Monte Carlo methods, Appl. Radiat. Isot. 68 (2010) 1231–1235.

[2] R. Breier, M. Laubenstein, P.P. Povinec, Monte Carlo simulation of background characteristics of a Ge detector operating underground in the Gran Sasso National Laboratory, Appl. Radiat. Isot. 126 (2016) 188–190.

[3] J. Ljungvall, J. Nyberg, A study of fast neutron interactions in high-purity germanium detectors, Nucl. Instrum. Methods Phys. Res. A 546 (2005) 553–573.

[4] E. Gete, D.F. Measday, B.A. Moftah, M.A. Saliba, T.J. Stocki, Neutron-induced peaks in ge detectors from evaporation neutrons, Nucl. Instrum. Methods Phys. Res. A 388 (1996) 212–219.

[5] K.W. Jones, H.W. Kraner, Stopping of 1- to 1.8-keV^{73}Ge atoms in germanium, Phys. Rev. C 4 (1971) 125–129.

[6] GEANT4 Collaboration, Introduction to Geant4, available at http://geant.cern.ch/. (Accessed 3 October 2017).

[7] S. Agostinelli, et al., Geant4 - a simulation toolkit, Nucl. Instrum. Methods Phys. Res. A 506 (2003) 250–303.

[8] J. Allison, et al., Geant4 developments and applications, IEEE Trans. Nucl. Sci. 53 (2006) 270–278.

[9] J. Allison, et al., Recent developments in geant4, Nucl. Instrum. Methods Phys. Res. A 835 (2016) 186–225.

[10] J. Scherzinger, R. Al Jebali, J.R.M. Annand, K.G. Fissum, R. Hall-Wilton, S. Koufigar, N. Mauritzson, F. Messi, H. Perrey, E. Rofors, A comparison of untagged gamma-ray and tagged-neutron yields from 241AmBe and 238PuBe sources, Appl. Radiat. Isot. 127 (2017) 98–102.

[11] D.V. Ellis, J.M. Singer, Well Logging for Earth Scientists, Springer, New York, 2007, pp. 325–382.

[12] Nuclear Data Center, Japan Atomic Energy Agency (JAEA), available at http://wwwndc.jaea.go.jp/jendl/j40/j40.html. (Accessed 3 October 2017).
[13] J.W. Marsh, D.J. Thomas, M. Burke, High resolution measurements of neutron energy spectra from Am-Be and Am-B neutron sources, Nucl. Instrum. Methods Phys. Res. A 366 (1995) 340–348.
[14] L.A. Sonzogni, National Nuclear Data Center, Brookhaven National Laboratory, available at https://www.nndc.bnl.gov/nudat2/https://www.nndc.bnl.gov/nudat2/. (Accessed 3 October 2017).
[15] D. Barker, W.Z. Wei, D.M. Mei, C. Zhang, Ionization efficiency study for low energy nuclear Recoils in Germanium, Astropart. Phys. 48 (2013) 8–15.
[16] L.G. Evans, P.N. Peplowski, E.A. Rhodes, D.J. Lawrence, T.J. McCoy, L.R. Nittler, S.C. Solomon, A.L. Sprague, K.R. Stockstill-Cahill, R.D. Starr, S.Z. Weider, W.V. Boynton, D.K. Hamara, J.O. Goldsten, Major-element abundances on the surface of Mercury: Results from the MESSENGER Gamma-Ray Spectrometer, J. Geophys. Res. 117 (2012) 1–14.
[17] M.M. Sternfelsa, F.A. Lowenheim, Tin plating from the potassium stannate bath, J. Electrochem. Soc. 82 (1942) 77–100.
[18] V.A. Kudryavtsev, L. Pandola, V. Tomasello, Neutron- and muon-induced background in underground physics experiments, Eur. Phys. J. A 36 (2008) 171–180.
[19] P.P. Povinec, M. Betti, A.J.T. Jull, New isotope technologies in environmental physics, Acta Phys. Slovaca 58 (1) (2008) 1–154.
[20] I. Murata, I. Tsuda, R. Nakamura, S. Nakayama, M. Matsumoto, H. Miyamar, Neutron and gamma-ray source-term characterization of AmBe sources in Osaka University, Progress Nucl. Sci. Tech. 4 (2014) 345–348.